Structural Perturbations Induced in Linear and Circular DNA by the Architectural Protein HU from *Bacillus stearothermophilus*†

James M. Benevides, Doinita Serban,‡ and George J. Thomas, Jr.*

School of Biological Sciences, University of Missouri—Kansas City, 5100 Rockhill Road, Kansas City, Missouri 64110-2499

Received November 17, 2005; Revised Manuscript Received February 17, 2006

ABSTRACT: HU is a small DNA-binding protein of eubacteria that is believed to induce or stabilize bending of the double helix and mediate nucleoid compaction in vivo. Although HU does not bind preferentially to specific DNA sequences, it is known to have high affinity for DNA sites containing structural anomalies, such as unpaired or mismatched bases, nicks, and four-way junctions. We have employed Raman spectroscopy to further investigate the structural basis of HU−DNA recognition in solution. Experiments were carried out on the homodimeric HU protein of *Bacillus stearothermophilus* (HUBst) and a 222-bp DNA fragment, which was isolated in linear (DNA^{L222}) and circular (DNA^{C222}) forms. In the absence of bound HUBst the Raman signatures of DNA^{L222} and DNA^{C222} are nearly superimposable, indicating that circularization produces no substantial change in the local B-DNA conformation. Conversely, the Raman signatures of DNA^{L222} and DNA^{C222} are perturbed significantly and specifically by HUBst binding. The HUBst-induced perturbations are markedly greater for the circularized DNA target. These results support an opportunistic molecular mechanism, in which HU binding is facilitated by intrinsic nonlinearity or flexibility in the DNA target. We propose that DNA segments which are bent or predisposed toward bending provide the high-affinity sites for HU attachment and nucleoid condensation. This model is consistent with the wide range of DNA bending angles reported in crystal structures of HU−DNA complexes.

The chromosomal DNA of eubacteria is associated with several small basic proteins in the highly condensed nucleoid structure (*1*, *2*). The most abundant component of all well-characterized eubacterial nucleoids is the histone-like protein HU (*3*, *4*), which occurs as an 18 kDa dimer (*5*). High-resolution structures of the homodimeric HU from *Bacillus stearothermophilus* (HUBst)[1] have been determined by both X-ray crystallography (*6*, *7*) and NMR spectroscopy (*8*). Structural studies of HU proteins from other eubacteria have been surveyed recently (*9*−*11*).

HU is structurally homologous to the eubacterial integration host factor (IHF), a heterodimeric DNA-binding protein that mediates interactions between DNA and other components of the nucleoid (*12*). Both sequence-specific and nonspecific modes of IHF/DNA recognition have been reported (*9*). Although the precise roles of HU and IHF in nucleoid formation remain unresolved (*2*), the two proteins have been shown to function similarly in reorganizing DNA topology to facilitate various gene regulatory functions (*13*−*17*). For example, in the case of phage λ genome recombination in *Escherichia coli*, HU can replace IHF by bending DNA and interacting equivalently with the recombinase protein, integrase. Interestingly, the eukaryotic high-mobility-group (HMG) box proteins HMG1 and HMG2 also appear to function nearly as effectively as HU and IHF in λ site-specific recombination (*18*). These results suggest common architectural roles for HU, IHF, and HMG-box proteins in manipulating the tertiary structure of DNA (*19*).

In contrast to IHF, which exhibits both specific and nonspecific DNA sequence recognition, the binding of HU to DNA is strictly sequence nonspecific, with K_d in the range of 200−2500 nM for B DNA (*20*). DNAs containing nicks, junctions, kinks, bends, or other alterations of the B-form structure can exhibit significantly more stable interactions with HU (K_d as low as 2 nM) (*1*, *21*, *22*). Distortions of the double helix may provide contacts for HU that are unavailable in undistorted B DNA. The affinities of binding of HU and other architectural proteins can be increased by circularization of the DNA target (*23*, *24*). This may reflect an energetic benefit associated with binding of the protein to a

† Paper 83 in the series Raman Spectral Studies of Nucleic Acids. Supported by National Institutes of Health Grant GM54378.

* To whom correspondence should be addressed. E-mail: thomasgj@umkc.edu. Telephone: 816-235-5247. Fax: 816-235-1503.

‡ Present address: The Scripps Research Institute, La Jolla, CA.

[1] Abbreviations: HUBst, HU protein from *Bacillus stearothermophilus*; IHF, integration host factor; HMG, high mobility group; DNA^{L222}, linear DNA consisting of a 222-bp duplex with complementary base triplet overhangs on the 5′ termini [sequence of the 5′-strand, (gtc)ctgcaacttt atccgcctcc atccagtcta ttaattgttg ccgggaagct agagtaagta gttcgccagt taatagtttg cgcaacgttg ttgccattgc tacaggcatc gtggtgtcac gctcgtcgtt tggtatggct tcattcagct ccggttccca acgatcaagg cgagttacat gatcccccat gtgtgcaaa aaagcggtta gctccttcg; molecular weight, 136.7 kDa; base composition, 50.4% AT and 49.6% GC]; DNA^{C222}, a 222-bp dsDNA circle, formed by ligation of DNA^{L222} (this nomenclature is employed for all circularized topoisomers of 222-bp DNA, irrespective of superhelical density); HEPES, *N*-(2-hydroxyethyl)piperazine-*N*′-2-ethanesulfonic acid; EtBr, ethidium bromide; AFM, atomic force microscopy.

10.1021/bi0523557 CCC: $33.50
Published on Web 04/04/2006

preformed recognition element; alternatively, circularization may impact protein binding by altering the transient fluctuations (dynamics) of linear B DNA.

Here we report a Raman spectroscopic analysis of the structural changes induced in a 222-bp DNA molecule upon binding of the homodomeric HU protein of *B. stearothermophilus*. Both linear and circular forms of the complexed DNA have been investigated. HUBst, which lacks both tyrosine and tryptophan residues and is therefore largely devoid of potentially interfering Raman bands from these aromatic amino acids, is well suited to sensitive Raman difference analysis of the structural perturbations induced in the protein-bound DNA (*25*, *26*). X-ray structures of uncomplexed HUBst (PDB accession number 1HUU) (*6*, *7*) have suggested a mechanism for DNA recognition in which the β-arms of the homodimer wrap around the DNA target and interact with the minor groove. The more recently published X-ray structure of a complex formed by the *Anabaena* HU dimer and a DNA oligomer supports this molecular mechanism and illustrates the bend induced in DNA by prolyl side chain intercalation (*27*). The induced-fit model is compatible with results of recent fluorescence resonance energy transfer studies (*28*) and provides the basis for interpreting the present Raman solution results.

Earlier, we reported Raman difference signatures diagnostic of diverse modes of protein−DNA recognition (*29*, *30*), including nonspecific recognition of dodecameric DNAs by HUBst (*26*). Such studies are facilitated by the rapid vibrational time scale of Raman spectroscopy, which permits detection of even short-lived protein−DNA complexes. The Raman spectral perturbations identified for HUBst−DNA complexes are consistent with nonspecific minor groove recognition, including modest bending of the helix axis (~70°), partial unstacking of bases, and reorganization of the DNA backbone. The present findings extend our earlier studies to a DNA target of transcriptionally relevant size in linear and circular forms.

MATERIALS AND METHODS

Expression and Purification of HUBst. HUBst was expressed in recombinant *E. coli* BL21(DE3)pLysS cells and purified as previously described (*25*, *31*). HUBst concentrations were determined by measurement of UV absorbance at 258 nm [$\epsilon_{258} = 0.076$ mL·mg^{-1}·cm^{-1} = 1482 M^{-1}·cm^{-1}] using a Cary 3E spectrophotometer (Varian, Inc., Palo Alto, CA) and assuming a subunit molecular mass of 9716 Da (*31*, *32*).

Preparation of Linear and Circular 222-bp DNA. E. coli strain DH5α containing the pUC19 plasmid in high copy number was purchased from Sigma Chemical Co. (St. Louis, MO) and purified as described (*33*). A linear 222-bp DNA sequence (DNA^{L222}) defined by *Ava*II restriction sites was excised from the purified plasmid using *Ava*II endonuclease obtained from New England Biolabs (Beverly, MA). DNA^{L222} was isolated from the digest by size exclusion chromatography on a Sephacryl S-500 column (2 × 90 cm) equilibrated with 100 mM NaCl and 10 mM Tris, pH 7.5, solution. The fractions containing DNA^{L222} were pooled and concentrated using an ultrafiltrator with 100 kDa cutoff (Centricon-100; Amicon, Inc., Beverly, MA). DNA concentrations were determined from absorbance measurements at 260 nm [ϵ_{260} = 13000 M (bp)$^{-1}$ cm^{-1}] (*34*).

Circular 222-bp DNA (DNA^{C222}) was prepared in a 150 mL reaction vial containing 3 μg/mL DNA^{L222}, 6 μg/mL HUBst, 50 mM HEPES (pH 7.5), 50 mM potassium glutamate, 10 mM $MgCl_2$, and 1 mM ATP. After incubation for 30 min at 30 °C, the end-joining reaction was initiated by the addition of 2000 units/mL T4 DNA ligase (New England Biolabs). After 30 min the contents of the reaction vial were transferred to a Centricon-100 ultrafiltrator and successively washed with 300 mL of 2 and 0.1 M NaCl solutions.

Electrophoresis. Samples of DNA^{L222} and DNA^{C222} were suspended at 40 μg/mL in electrophoresis buffer (20 mM Tris−acetate, 20 mM sodium acetate, 1 mM EDTA) and run for 1.5 h at 4 °C on gels containing 3% Nusieve agarose (Cambrex Bio Science Walkersville, Inc., Walkersville, MD) and 1% electrophoresis grade agarose. These runs effectively distinguished linear and circular forms of 222-bp DNA. To further distinguish different circular forms that may result from the influence of HUBst (*35*), DNA^{C222} was run on 2% agarose gels containing 0.5 μg/mL ethidium bromide (EtBr), 10 mM Tris (pH 8.0), and 1 mM EDTA. Open circles were distinguished from covalently closed circles by heating the solution of circular DNA to 95 °C for 2 min and rapidly cooling to −70 °C prior to electrophoresis on the same 2% agarose/EtBr gel.

Complexes of DNA and HUBst in sample buffer (50 mM NaCl, 10 mM Tris, pH 7.5), prepared with different molar ratios of protein dimer to 222-bp nucleic acid (in the range 4.5:1 to 40:1), were also examined on agarose gels. The appropriate mixtures of HUBst and DNA, typically in 10 μL total volume, were incubated at 20 °C for 15 min prior to being loaded on the gel. A 2 μL aliquot of dye solution (15% glycerol, 0.05% bromophenol blue) was added to each sample. Samples were applied to 4% composite agarose gels (described above) that had been prerun for 30 min at 110 V and 4 °C and subsequently run at the same voltage and temperature for 4 h. DNA was visualized by staining with EtBr (*34*) and quantified using Quantity One software (Bio-Rad Laboratories, Inc., version 4.4.0.). The fractions of unbound and protein-bound DNA in a given lane were determined from the integrated band areas, and the total amount of DNA in each lane was computed from the sum of band areas.

Atomic Force Microscopy. Mica surfaces were treated for 5 min with a suspension containing one part of 3-aminopropyltriethoxysilane (Sigma Chemical Co.) in 10000 parts of water. The mica surfaces were then rinsed with water and dried under a filtered argon stream. DNA solutions (0.5 μg/mL in 0.1 mM Tris, pH 8.0) were pipetted onto the mica surface and allowed to stand for at least 10 min at ambient temperature. The mica surface was again dried with filtered argon prior to scanning. Atomic force microscopy (AFM) imaging was carried out at the University of Alabama, Birmingham, in the laboratory of Dr. Rigoberto C. Advincula, using a scanning microscope (PicoSPM; Molecular Imaging, Phoenix, AZ) equipped with an 8 × 8 μm scanner. Images were obtained by scanning with a magnetic AC drive (MacMode) using silicon MAC levers of nominal spring constant (0.6 N/m). The free operating amplitude was set at 5 nm point to point with a 10% reduction set point. The drive frequency was 25 kHz. Images were analyzed using

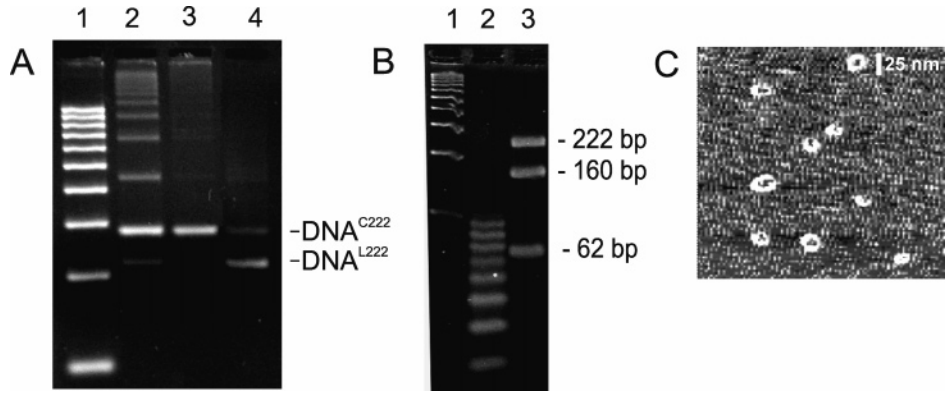

FIGURE 1: Electrophoretic analysis of the ligation products of linear 222-bp DNA (DNA^{L222}). Panel A: lane 1, 100-bp DNA ladder; lane 2, products of T4 ligase treatment of HUBst-bound DNA^{L222}, yielding circularized monomer, DNA^{C222}, plus higher order concatemers; lane 3, digestion of the lane 2 products with exonuclease III and proteinase K, yielding purified DNA^{C222} that is free of bound HUBst; lane 4, product of digestion of DNA^{C222} with restriction endonuclease *Bsp*L1, which restores a linear 222-bp form. Panel B: lane 1, 100-bp DNA ladder; lane 2, 10-bp DNA ladder; lane 3, DNA^{L222} partially digested with *Bsp*L1, yielding 160 and 62-bp fragments (cf. panel A, lane 4). Panel C: AFM image of DNA^{C222}.

NIH Image software (Molecular Imaging Corp., Phoenix, AZ).

Raman Spectroscopy. Raman spectra were collected from solutions of HUBst (20 μg/μL $\approx$ 1 mM dimer), DNA^{L222} and DNA^{C222} (40 μg/μL $\approx$ 0.29 mM duplex), and their corresponding 20:1 molar complexes (HUBst−DNA) in sample buffer. The complexes were prepared by dissolving the appropriate weight of lyophilized protein in 0.29 mM DNA solution. Aliquots ($\sim$5 μL) were sealed in glass capillaries (KIMAX no. 34507), mounted in the sample illuminator of the Raman spectrophotometer, and thermostated at 20 °C (*36*). Spectra were excited at 532 nm using a solid-state Nd:YVO_4 laser (Verdi; Coherent, Inc., Santa Clara, CA). Raman scattering at 90° was collected on a Spex 500M single spectrograph (Instruments S.A., Edison, NJ), equipped with a holographic notch filter and liquid nitrogen cooled, back-thinned, charge-coupled-device detector of 2000 $\times$ 800 pixels (Spectrum One, Instruments S.A.). The radiant power at the sample was approximately 80 mW. The effective spectral resolution was 3 cm^{-1}. Raman frequencies, accurate to $\pm$0.5 cm^{-1}, were calibrated using the 459.5 cm^{-1} band of CCl_4. Spectra presented below are the accumulated averages of 10−30 exposures of 40 s each. Further details of the instrumentation and data collection protocols are given elsewhere (*37*). Raman difference peaks and troughs that represent at least 5% of the parent band intensity and have a signal-to-noise ratio of at least 2:1 are judged to be experimentally significant.

RESULTS AND INTERPRETATION

Effect of HUBst on Ligation of 222-bp DNA. Lane 2 of Figure 1A shows a multiplicity of products resulting from the ligation of DNA^{L222} with T4 ligase in the presence of HUBst. When the products of this ligation reaction are subsequently incubated with exonuclease III and proteinase K, the gel is dominated by a single species that is free of bound HUBst (lane 3). Purification and treatment of this DNA product with *Bsp*L1 (Figure 1A, lane 3), which is expected to cleave between the base pairs that correspond to positions 62 and 63 of DNA^{L222}, yield a species with the same electrophoretic mobility as DNA^{L222} (Figure 1A, lane 4). These results are consistent only with a covalently closed

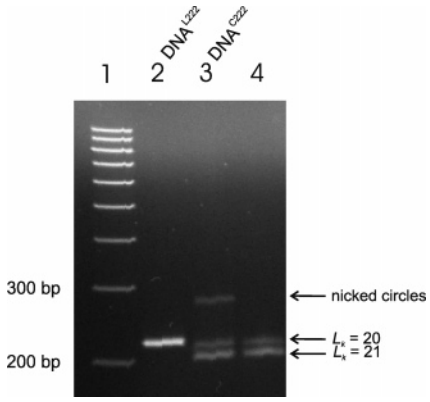

FIGURE 2: Resolution of DNA^{C222} topoisomers in EtBr-containing gel. Lanes: 1, 100-bp DNA ladder; 2, DNA^{L222}; 3, DNA^{C222} topoisomer distribution, as labeled; 4, DNA^{C222} topoisomer distribution after 5 min at 95 °C and rapid cooling to −70 °C.

monomeric DNA circle (DNA^{C222}) as the major product of the T4 ligation reaction. Lanes 3 and 4 of Figure 1A thus provide a comparison of the distinct electrophoretic mobilities of DNA^{C222} and DNA^{L222}, respectively, in 4% agarose. Figure 1B shows that further treatment of DNA^{L222} with *Bsp*L1 yields the anticipated 160-bp and 62-bp fragments, while additional confirmation of the circular topology of the DNA^{C222} construct (Figure 1A, lane 3) is provided by atomic force microscopy (AFM) images (Figure 1C).

It is important to note that the ligation of linear 222-bp DNA in the presence of HUBst may produce either nicked circles, nonnicked but relaxed circles (linking number, L_k^0 = 222/10.4 = 21), or negative supercoils ($L_k < L_k^0$) (*35*). Although such different topoisomers of DNA^{C222} cannot be resolved by electrophoresis in pure agarose gels (Figure 1A), they are rendered distinguishable by including an intercalant such as EtBr in the gel medium. EtBr facilitates discrimination of DNA^{C222} topoisomers by induction of positive supercoiling in nonnicked species. This is evident in the agarose/EtBr gel profile of DNA^{C222} shown in Figure 2 (lane 3), where three distinct subbands become resolved. The relative intensities (from top to bottom) correspond roughly to 17%:33%:50% of the cumulative intensity. The least abundant and slowest migrating species is readily assigned to nicked circles (cf. Figure 1A); i.e., EtBr binding cannot induce supercoiling of this DNA species. This is consistent

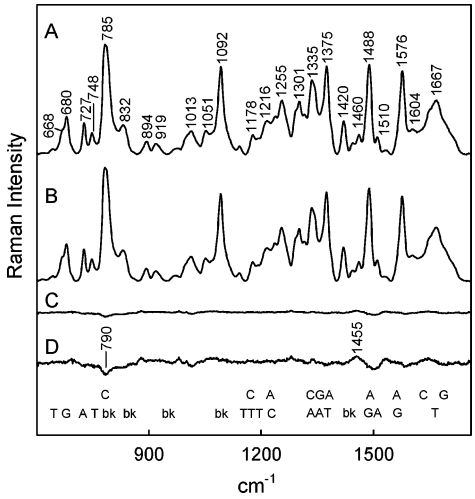

FIGURE 3: Raman spectra (600−1800 cm^{-1}, 532 nm excitation) of DNA^{C222} (A) and DNA^{L222} (B), each at 40 $\mu g/\mu L$ in 150 mM NaCl, pH 7.5, solution, and their difference spectra (C = A − B). A 3-fold amplification of the difference spectrum is also shown (D). (A), (B), and (C) were normalized to the integrated intensity of the band at 1092 cm^{-1}, which is independent of base composition (*45*). Assignments of the principal bands to base (A, C, T, G) or backbone vibrations (bk) are indicated.

with the fact that heating DNA^{C222} followed by rapid cooling, which selectively degrades nicked circles, eliminates only the slowest migrating species (Figure 2, lane 4) (*23*). The two more rapidly migrating species are distinct topoisomers, which reflect the net effect of HUBst-induced negative supercoiling during covalent closure and EtBr-induced positive supercoiling in the agarose/EtBr gel medium. In vitro measurements have established that with HU binding L_k is decreased by approximately 1.0 per 290 bp (*35*, *38*). Therefore, in addition to circles with $L_k^0 = 21$, circles with $L_k = 20$ are also expected to be produced when circularization is carried out in the presence of HUBst. The topoisomer that has the lower L_k value in the absence of intercalant will also have the lower L_k in the agarose/EtBr gel, since a fraction of the intercalant will be required to relax any negative supercoils already present. Hence, the topoisomer with $L_k = 20$ will have one less positive supercoil in the agarose/EtBr gel than the topoisomer with $L_k = 21$. The more prevalent topoisomer, which is the most highly supercoiled because it exhibits the fastest migration in the agarose/EtBr gel shown in Figure 2, can be assigned on the basis of the above considerations to the topoisomer with $L_k = 21$. The intermediate band is by default assigned to the topoisomer with $L_k = 20$.

The AFM images of DNA^{C222} presented in Figure 1C (and additional images not shown) do not readily resolve the three topoisomers distinguished by agarose/EtBr electrophoresis. This may be due in part to both the low salt conditions (*39*) required for effective AFM imaging and very low superhelical densities of the topoisomers ($L_k = 20, 21$).

Raman Signatures of Linear and Circular 222-bp DNA. Raman spectra of DNA^{C222} and DNA^{L222} are presented in traces A and B, respectively, of Figure 3. Labels identify prominent Raman bands of the DNA bases (A, T, G, C) and backbone (bk) on the basis of previously developed assignments (*40*−*46*). Subtraction of the two (A − B) yields the nearly null difference spectrum shown in trace C (normalized to the parent spectral intensity and amplified 3-fold in trace D). Figure 3 shows that DNA^{C222} and DNA^{L222} have very similar B conformations, as evidenced by Raman markers of C2′-*endo/anti* dG (680 cm^{-1}), dA (727 cm^{-1}), and dT (748 cm^{-1}) deoxynucleosides and by *gauche*$^-$ (g^-) conformations of phosphodiester torsions α and ζ (790 and 832 cm^{-1}). Raman difference bands in trace C (or as amplified in trace D) that meet the criteria for significance (see Materials and Methods section, above) occur at 790 and 1455 cm^{-1}. These are assigned to vibrational modes of the deoxyribosyl phosphate moiety (*47*).

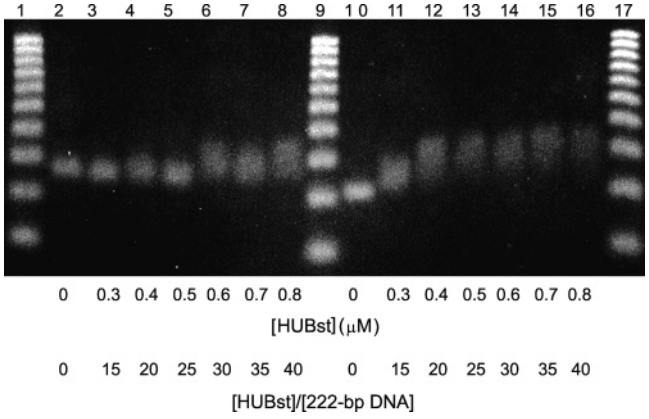

FIGURE 4: Gel mobility shift assay of complexes formed in mixtures of HUBst with 222-bp DNAs (DNA^{C222}, lanes 2−8, and DNA^{L222}, lanes 10−16). The DNA concentration in each lane is 20 nM. HUBst concentrations (μM) and HUBst:DNA molar ratios are as indicated below the gel. Further details are discussed in the text. Lanes 1, 9, and 17 contain a 100−1000-bp DNA ladder.

Electrophoretic Characterization of HUBst−DNA Complexes. The stoichiometry of HUBst binding to DNA^{C222} and DNA^{L222} was investigated by gel mobility shift assay (Figure 4) with a constant concentration of DNA (0.03 μM) and increasing concentrations of HUBst dimer, ranging from 0.3 to 0.8 μM. For complexes of both the circular (DNA^{C222}, lanes 3−8) and linear (DNA^{L222}, lanes 11−16) molecules, the electrophoretic mobilities are distinct from those of the corresponding protein-free DNAs.

For example, in the case of the DNA^{L222} complexes, DNA mobility *decreases* with increasing HUBst dimer concentration up to a protein-to-DNA ratio of about 25:1. The resulting complex presumably contains on average one HUBst dimer bound per DNA^{L222} molecule. Upon further increasing the ratio of HUBst to DNA^{L222}, the stoichiometry of binding increases until saturation is achieved. Although the stoichiometry of binding at saturation is not known, we expect a maximum of one HUBst dimer bound per 11−15 bp (*35*, *48*). In the case of DNA^{C222} complexes, mobility *increases* slightly with increasing HUBst concentration up to an approximate HUBst:DNA^{C222} ratio of 25:1 (Figure 4, lanes 3−5), which contrasts with the retardation in electrophoretic mobility observed for the linear DNA molecule (Figure 4, lanes 13−16). The increased electrophoretic mobility of the HUBst−DNA^{C222} complex can be attributed to a more compact shape than occurs for the protein-free circle. A similar mobility increase has been observed for circular DNA complexes of the archaebacterial HU analogue, MC1 (*49*).

Figure 4 also shows that at protein-to-DNA ratios below saturation the bands of the HUBst−DNA^{C222} complex (lanes 3−5) are sharper than those of the HUBst−DNA^{L222} complex (lanes 11−13), consistent with tighter binding of HUBst to

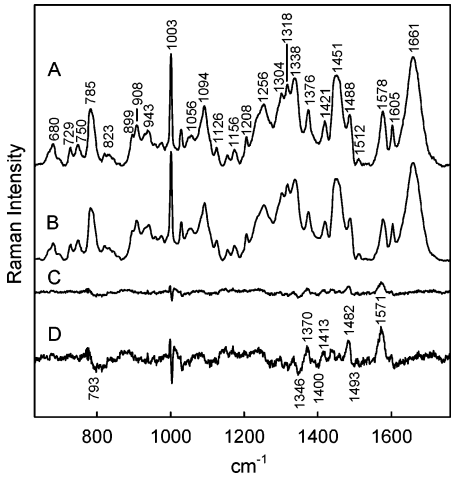

FIGURE 5: (A) Raman spectrum (600−1800 cm^{-1}, 532 nm excitation) of the HUBst−DNA^{L222} complex (20:1 molar ratio). (B) Spectral sum of constituents (HUBst + DNA). (C) Computed difference spectrum (A − B). (D) Threefold amplification of (C). The complex was prepared by adding the appropriate aliquot of lyophilized protein solution (20 $\mu g/\mu L \approx 1$ mM dimer) to the DNA solution (40 $\mu g/\mu L \approx 0.29$ mM). Samples were thermostated at 20 °C.

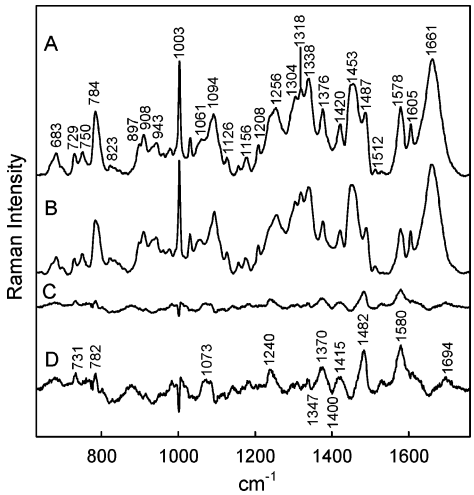

FIGURE 6: (A) Raman spectrum (600−1800 cm^{-1}, 532 nm excitation) of the HUBst−DNA^{C222} complex (20:1 molar ratio). (B) Spectral sum of constituents (HUBst + DNA). (C) Computed difference spectrum (A − B). (D) Threefold amplification of (C). Other conditions are as given in Figure 5. Comparison of trace D with its counterpart in Figure 5 illustrates the more pronounced spectral differences attendant with formation of the HUBst−DNA^{C222} complex.

the circular target. Enhanced binding affinity of HUBst for DNA^{C222} is also supported by a competitive gel shift assay (Figure S1, available as Supporting Information).

Raman Analysis of HUBst−DNA Complexes. In Figure 5 the Raman spectrum of HUBst−DNA^{L222} (trace A) is compared with the spectral sum of constituents (trace B). The computed difference spectrum (complex minus sum, trace C) is amplified 3-fold (trace D) to reveal a number of small but significant perturbations in Raman bands assignable to DNA. Corresponding data for the HUBst−DNA^{C222} complex are shown in Figure 6. In the difference spectra of Figures 5 and 6, only the peaks and troughs that meet the criteria for significance are labeled (see Materials and Methods). The results show clearly that HUBst binding alters the structures of both the linear and circular 222-bp DNA targets. The similar pattern of peaks and troughs in both difference spectra also indicates that both DNAs undergo similar structural rearrangements with HUBst binding. However, the difference bands of DNA^{C222} generally exhibit greater amplitudes, which suggests that the structure of the circular target is more significantly perturbed by HUBst binding. Because all of the prominent difference features of Figures 5 and 6 are assignable to DNA, we conclude further that the solution structure of HUBst is largely conserved with DNA interaction.

The common pattern of difference peaks and troughs in the 770−860 cm^{-1} interval of Figures 5 and 6 implies that HUBst induces similar conformational reorganizations in the phosphodiester networks (C5′−O5′−P−O3′−C3′) of DNA^{L222} and DNA^{C222}. This difference spectral signature is similar to that reported previously for the binding of HUBst to dodcameric DNAs, although the magnitudes of the perturbations here (∼7%) are less than those observed previously (∼33%) (*26*). This is consistent with the relatively low HUBst binding stoichiometry for 222-bp DNA vis-à-vis dodecameric DNA. The difference peak near 1415 cm^{-1}, which is common to both linear and circular complexes and is attributable in both cases to a Raman marker of the deoxyribosyl moiety (*47*), provides additional evidence for HUBst-induced perturbation of DNA backbone geometry. The 1415 cm^{-1} difference feature has been identified previously as a marker of minor groove recognition (*29*).

The prominent difference peaks near 1370, 1482, and 1575 cm^{-1} in Figures 5 and 6 identify altered DNA base environments in the complexes. The latter two peaks may reflect recovery of Raman hypochromism accompanying partial unstacking of purines (*43*, *50*, *51*). These effects are again more pronounced for the DNA^{C222} than for the DNA^{L222} complex, which also shows greater differences for the stacking-sensitive markers of dA and dT at 731 and 1240 cm^{-1}, respectively (Figure 6) (*37*). Thymine residues of B DNA also generate a marker near 1370−1375 cm^{-1}, which is known to exhibit intensity enhancement with increasing hydrophobicity of the local environment of the $C5H_3$ group (*52*). Accordingly, we attribute the difference peak at 1370 cm^{-1} in Figures 5 and 6 to increased hydrophobicity of thymine $C5H_3$ environments in the complexes. A similar effect has been observed for HUBst complexes of dodecameric DNAs (*26*).

DISCUSSION AND CONCLUSIONS

The Raman signatures of linear and circular variants of 222-bp DNA are nearly superposable, as evidenced by the absence of prominent features in the difference spectrum of Figure 3C. Even 3-fold amplification of this difference spectrum (Figure 3D) reveals very weak difference bands, indicating only small local conformational changes with circularization. The spectral bands principally affected (790, 1455 cm^{-1}) are due to vibrations of the sugar−phosphate backbone (*33*, *47*, *53*, *54*). The nearly negligible effect of circularization on the Raman signature of the linear DNA investigated here is not surprising in view of the small average bending angle associated with closing a circle of 222 base pairs (∼1.7°/bp or 16°/turn). This is close to the experimentally determined consensus value for static curvature of an A-tract DNA duplex (∼18°/turn) (*55*).

As noted above (Figure 2 and related discussion), up to one-third of the present DNA^{C222} construct may consist of negative supercoils. However, the low level of supercoiling ($\sigma = -0.05$) perturbs the DNA Raman signature only marginally (*33*). Hence, the bending of DNA^{C222} by 1.7°/bp is considered to be the principal source of the Raman difference bands of Figure 3C. These results contrast strikingly with the much larger effects of protein-induced DNA curvature (*26*, *29*, *52*, *56*). The latter perturbations are characterized by both shifts in wavenumber values and changes in amplitudes affecting numerous Raman bands, including several that are diagnostic of specific base interactions. Interestingly, both circularization and protein-induced curvature generate a distinctive Raman difference band at 1460 cm^{-1}. We have assigned this difference feature to a change in the local environment of the deoxyribosyl C5′H_2 groups (*29*).

Raman difference spectra for solutions of both the HUBst−DNA^{L222} (Figure 5D) and HUBst−DNA^{C222} (Figure 6D) complexes reveal appreciable base unstacking as well as reorganization of the DNA backbone with HUBst binding. The pattern of perturbed Raman marker bands is similar for the two complexes. It also shares many similarities with the difference pattern reported previously for HUBst binding to dodecameric DNA (*26*). Thus, the variants of 222-bp DNA (linear and circular) and 12-bp DNA (sequence isomers) employ a common HUBst recognition mechanism. On the basis of available crystal structures (*27*), the mechanism is presumed to involve minor groove widening and a localized network of electrostatic interactions in the bent DNA.

Despite the similar patterns of perturbed Raman bands in Figures 5D and 6D, the HUBst−DNA^{L222} and HUBst−DNA^{C222} complexes are distinguished by the fact that the difference bands have markedly greater amplitudes in the latter case. This is especially evident for bands that are diagnostic of base stacking. For example, the more intense positive difference features (hyperchromism) at 1240 (dT), 731 (dA), 1482 (dG, dA), and 1580 (dA, dG) cm^{-1} indicate greater unstacking of pyrimidines and purines in the HUBst−DNA^{C222} complex. The enhanced electrophoretic mobility of HUBst−DNA^{C222} relative to HUBst−DNA^{L222} at low binding ratios (Figure 4) also supports this conclusion.

The electrophoretic mobility of HUBst−DNA^{C222} is also enhanced relative to that of protein-free DNA^{C222} (Figure 4). We attribute this diminished hydrodynamic volume of HUBst−DNA^{C222} to protein-induced compaction of the DNA^{C222} target. Such compaction, which presumably reflects the formation of a small number of bends or kinks at the loci of HUBst binding, is considered analogous to that reported for binding of the MC1 protein of *Methanosarcinaceae* to a 207-bp circular DNA target (*49*). It has been suggested that the binding of HU proteins to DNA at low protein-to-DNA ratios increases DNA flexibility and facilitates nucleoid formation (*2*). While our results do not address the relevance of HUBst-induced compaction of DNA^{C222} to nucleoid-like complexes, we regard the electrophoretic properties of the HUBst−DNA^{C222} structure as incompatible with increased DNA flexibility.

The present results show that HUBst exhibits greater binding affinity for DNA^{C222} than DNA^{L222}. This is consistent with studies of the architectural proteins IHF (*23*, *57*), MC1 (*49*), and HMG1 (*24*, *58*), which show that circularization of the DNA target enhances binding affinity. Limiting the conformational space accessible to DNA via circularization apparently reduces the thermodynamic cost of sharply bending the double helix (*23*). *Our data demonstrate further that the circularized DNA target* (DNA^{C222}) *suffers more extensive structural reorganization than its linear counterpart* (DNA^{L222}). Evidently, DNA circularization not only enhances HU binding affinity but also extends the locus of HU−DNA interaction to include additional base pairs that do not otherwise participate (presumably those adjoining the minor groove intercalation site). The occurrence of additional protein−DNA contacts specific to the HUBst−DNA^{C222} complex suggests a parallel to recently reported HUBst−DNA crystal structures (*11*, *27*), where more extensive protein−DNA interactions are observed when the DNA target is modified to facilitate wrapping along the protein surface. In the present case, interaction is favored by the intrinsic curvature of the 222-bp DNA circle.

The results of this work suggest that HU functions opportunistically to stabilize bent regions of DNA and to manipulate relatively flexible segments of DNA, rather than to introduce curvature de novo in unbent or rigid DNA.

ACKNOWLEDGMENT

The authors thank Marta Kozbial and Jessica Kawakami for expert technical assistance.

SUPPORTING INFORMATION AVAILABLE

TBE gel (4−20%) showing the results of competitive binding of HUBst for DNA^{C222} and DNA^{L222} (Figure S1). This material is available free of charge via the Internet at http://pubs.acs.org.

REFERENCES

1. Grove, A., and Lim, L. (2001) High-affinity DNA binding of HU protein from the hyperthermophile *Thermotoga maritima*, *J. Mol. Biol. 311*, 491−502.
2. Dame, R. T., and Goosen, N. (2002) HU: Promoting or counteracting DNA compaction?, *FEBS Lett. 529*, 151−156.
3. Shellman, V. L., and Pettijohn, D. E. (1991) Introduction of proteins into living bacterial cells: Distribution of labeled HU protein in *Escherichia coli*, *J. Bacteriol. 173*, 3047−3059.
4. Kulyba, N. P., and Kozlov, A. V. (1989) Level of HU protein binding with DNA and the HU/DNA ratio in *Escherichia coli* cells with various generation periods, *Biokhimiya 54*, 1075−1081.
5. Drlica, K., and Rouviere-Yaniv, J. (1987) Histonelike proteins of bacteria, *Microbiol. Rev. 51*, 301−319.
6. White, S. W., Appelt, K., Wilson, K. S., and Tanaka, I. (1989) A protein structural motif that bends DNA, *Proteins 5*, 281−288.
7. White, S. W., Wilson, K. S., Appelt, K., and Tanaka, I. (1999) The high-resolution structure of DNA-binding protein HU from *Bacillus stearothermophilus*, *Acta Crystallogr., Sect. D: Biol. Crystallogr. 55* (Part 4), 801−809.
8. Boelens, R., Vis, H., Vorgias, C. E., Wilson, K. S., and Kaptein, R. (1996) Structure and dynamics of the DNA binding protein HU from *Bacillus stearothermophilus* by NMR spectroscopy, *Biopolymers 40*, 553−559.
9. Rice, P. A. (1997) Making DNA do a U-turn: IHF and related proteins, *Curr. Opin. Struct. Biol. 7*, 86−93.
10. Christodoulou, E., Rypniewski, W. R., and Vorgias, C. R. (2003) High-resolution X-ray structure of the DNA-binding protein HU from the hyper-thermophilic *Thermotoga maritima* and the determinants of its thermostability, *Extremophiles 7*, 111−122.
11. Swinger, K. K., and Rice, P. A. (2004) IHF and HU: Flexible architects of bent DNA, *Curr. Opin. Struct. Biol. 14*, 28−35.
12. Rice, P. A., Yang, S., Mizuuchi, K., and Nash, H. A. (1996) Crystal structure of an IHF-DNA complex: A protein-induced DNA U-turn, *Cell 87*, 1295−1306.

13. Kahn, J. D. (2000) Topological effects of the TATA box binding protein on minicircle DNA and a possible thermodynamic linkage to chromatin remodeling, *Biochemistry 39*, 3520−3524.
14. Balandina, A., Claret, L., Hengge-Aronis, R., and Rouviere-Yaniv, J. (2001) The *Escherichia coli* histone-like protein HU regulates rpoS translation, *Mol. Microbiol. 39*, 1069−1079.
15. Kow, Y. W., Imhoff, B., Ali, M. M., and Hashimoto, M. (2003) HU protein of *Escherichia coli* has a role in the repair of closely opposed lesions in DNA, *J. Biol. Chem. 278*, 28501−28507.
16. Aki, T., and Adhya, S. (1997) Repressor induced site-specific binding of HU for transcriptional regulation, *EMBO J. 16*, 3666−3674.
17. Lyubchenko, Y. L., Shlyakhtenko, L. S., Aki, T., and Adhya, S. (1997) Atomic force microscopic demonstration of DNA looping by GalR and HU, *Nucleic Acids Res. 25*, 873−876.
18. Segall, A. M., Goodman, S. D., and Nash, H. A. (1994) Architectural elements in nucleoprotein complexes: Interchangeability of specific and non-specific DNA binding proteins, *EMBO J. 13*, 4536−4548.
19. Travers, A. (2000) Recognition of distorted DNA structures by HMG domains, *Curr. Opin. Struct. Biol. 10*, 102−109.
20. Kamashev, D., and Rouviere-Yaniv, J. (2000) The histone-like protein HU binds specifically to DNA recombination and repair intermediates, *EMBO J. 19*, 6527−6535.
21. Kamashev, D., Balandina, A., and Rouviere-Yaniv, J. (1999) The binding motif recognized by HU on both nicked and cruciform DNA, *EMBO J. 18*, 5434−5444.
22. Castaing, B., Zelwer, C., Laval, J., and Boiteux, S. (1995) HU protein of *Escherichia coli* binds specifically to DNA that contains single-strand breaks or gaps, *J. Biol. Chem. 270*, 10291−10296.
23. Teter, B., Goodman, S. D., and Galas, D. J. (2000) DNA bending and twisting properties of integration host factor determined by DNA cyclization, *Plasmid 43*, 73−84.
24. Webb, M., Payet, D., Lee, K. B., Travers, A. A., and Thomas, J. O. (2001) Structural requirements for cooperative binding of HMG1 to DNA minicircles, *J. Mol. Biol. 309*, 79−88.
25. Serban, D., Arcineigas, S. F., Vorgias, C. E., and Thomas, G. J., Jr. (2003) Structure and dynamics of the DNA-binding protein HU of *B. stearothermophilus* investigated by Raman and ultraviolet-resonance Raman spectroscopy, *Protein Sci. 12*, 861−870.
26. Serban, D., Benevides, J. M., and Thomas, G. J., Jr. (2003) HU protein employs similar mechanisms of minor-groove recognition in binding to different B-DNA sites: Demonstration by Raman spectroscopy, *Biochemistry 42*, 7390−7399.
27. Swinger, K. K., Lemberg, K. M., Zhang, Y., and Rice, P. A. (2003) Flexible DNA bending in HU-DNA cocrystal structures, *EMBO J. 22*, 3749−3760.
28. Wojtuszewski, K., and Mukerji, I. (2003) HU binding to bent DNA: A fluorescence resonance energy transfer and anisotropy study, *Biochemistry 42*, 3096−3104.
29. Benevides, J. M., Chan, G., Lu, X. J., Olson, W. K., Weiss, M. A., and Thomas, G. J., Jr. (2000) Protein-directed DNA structure. I. Raman spectroscopy of a high-mobility-group box with application to human sex reversal, *Biochemistry 39*, 537−547.
30. Benevides, J. M., Li, T., Lu, X. J., Srinivasan, A. R., Olson, W. K., Weiss, M. A., and Thomas, G. J., Jr. (2000) Protein-directed DNA structure II. Raman spectroscopy of a leucine zipper bZIP complex, *Biochemistry 39*, 548−556.
31. Padas, P. M., Wilson, K. S., and Vorgias, C. E. (1992) The DNA-binding protein HU from mesophilic and thermophilic bacilli: Gene cloning, overproduction and purification, *Gene 117*, 39−44.
32. Welfle, H., Misselwitz, R., Welfle, K., Groch, N., and Heinemann, U. (1992) Salt-dependent and protein-concentration-dependent changes in the solution structure of the DNA-binding histone-like protein, HBsu, from *Bacillus subtilis*, *Eur. J. Biochem. 204*, 1049−1055.
33. Serban, D., Benevides, J. M., and Thomas, G. J., Jr. (2002) DNA secondary structure and Raman markers of supercoiling in *Escherichia coli* plasmid pUC19, *Biochemistry 41*, 847−853.
34. Sambrook, J., Fritsch, E. F., and Maniatis, T. (1989) *Molecular Cloning: A Laboratory Manual*, Cold Spring Harbor Laboratory Press, Cold Spring Harbor, NY.
35. Broyles, S. S., and Pettijohn, D. E. (1986) Interaction of the *Escherichia coli* HU protein with DNA. Evidence for formation of nucleosome-like structures with altered DNA helical pitch, *J. Mol. Biol. 187*, 47−60.
36. Thomas, G. J., Jr., and Barylski, J. (1970) Thermostating capillary cells for a laser-Raman spectrophotometer, *Appl. Spectrosc. 24*, 463−464.
37. Movileanu, L., Benevides, J. M., and Thomas, G. J. (1999) Temperature dependence of the Raman spectrum of DNA. I. Raman signatures of premelting and melting transitions of poly(dA-dT)·poly(dA-dT), *J. Raman Spectrosc. 30*, 637−649.
38. Tanaka, H., Yasuzawa, K., Kohno, K., Goshima, N., Kano, Y., Saiki, T., and Imamoto, F. (1995) Role of HU proteins in forming and constraining supercoils of chromosomal DNA in *Escherichia coli*, *Mol. Gen. Genet. 248*, 518−526.
39. Bednar, J., Furrer, P., Stasiak, A., Dubochet, J., Egelman, E. H., and Bates, A. D. (1994) The twist, writhe and overall shape of supercoiled DNA change during counterion-induced transition from a loosely to a tightly interwound superhelix. Possible implications for DNA structure *in vivo*, *J. Mol. Biol. 235*, 825−847.
40. Lord, R. C., and Thomas, G. J., Jr. (1967) Raman spectral studies of nucleic acids and related molecules. I. Ribonucleic acid derivatives, *Spectrochim. Acta 23A*, 2551−2591.
41. Erfurth, S. C., Kiser, E. J., and Peticolas, W. L. (1972) Determination of the backbone structure of nucleic acids and nucleic acid oligomers by laser Raman scattering, *Proc. Natl. Acad. Sci. U.S.A. 69*, 938−941.
42. Erfurth, S. C., and Peticolas, W. L. (1975) Melting and premelting phenomenon in DNA by laser Raman scattering, *Biopolymers 14*, 247−264.
43. Prescott, B., Steinmetz, W., and Thomas, G. J., Jr. (1984) Characterization of DNA structures by laser Raman spectroscopy, *Biopolymers 23*, 235−256.
44. Benevides, J. M., Wang, A. H. J., van der Marel, G. A., van Boom, J. H., and Thomas, G. J., Jr. (1988) Crystal and solution structures of the *B*-DNA dodecamer d(CGCAAATTTGCG) probed by Raman spectroscopy: Heterogeneity in the crystal structure does not persist in the solution structure, *Biochemistry 27*, 931−938.
45. Deng, H., Bloomfield, V. A., Benevides, J. M., and Thomas, G. J., Jr. (1999) Dependence of the Raman signature of genomic B-DNA on nucleotide base sequence, *Biopolymers 50*, 656−666.
46. Movileanu, L., Benevides, J. M., and Thomas, G. J., Jr. (2002) Temperature dependence of the Raman spectrum of DNA. II. Raman signatures of premelting and melting transitions of poly(dA)·poly(dT) and comparison with poly(dA-dT)·poly(dA-dT), *Biopolymers 63*, 181−194.
47. Thomas, G. J., Jr., Benevides, J. M., Overman, S. A., Ueda, T., Ushizawa, K., Saitoh, M., and Tsuboi, M. (1995) Polarized Raman spectra of oriented fibers of A DNA and B DNA: Anisotropic and isotropic local Raman tensors of base and backbone vibrations, *Biophys. J. 68*, 1073−1088.
48. Shindo, H., Furubayashi, A., Shimizu, M., Miyake, M., and Imamoto, F. (1992) Preferential binding of *E. coli* histone-like protein HU α to negatively supercoiled DNA, *Nucleic Acids Res. 20*, 1553−1558.
49. Toulme, F., Le Cam, E., Teyssier, C., Delain, E., Sautiere, P., Maurizot, J. C., and Culard, F. (1995) Conformational changes of DNA minicircles upon the binding of the archaebacterial histone-like protein MC1, *J. Biol. Chem. 270*, 6286−6291.
50. Small, E. W., and Peticolas, W. L. (1971) Conformational dependence of the Raman scattering intensities from polynucleotides, *Biopolymers 10*, 69−88.
51. Benevides, J. M., Stow, P. L., Ilag, L. L., Incardona, N. L., and Thomas, G. J., Jr. (1991) Differences in secondary structure between packaged and unpackaged single-stranded DNA of bacteriophage φX174 determined by Raman spectroscopy: A model for φX174 DNA packaging, *Biochemistry 30*, 4855−4863.
52. Benevides, J. M., Weiss, M. A., and Thomas, G. J., Jr. (1991) DNA recognition by the helix-turn-helix motif: Investigation by laser Raman spectroscopy of the phage λ repressor and its interaction with operator sites O_L1 and O_R3, *Biochemistry 30*, 5955−5963.
53. Tsuboi, M., Komatsu, K., Hoshi, J., Kawashima, E., Sekine, T., Ishido, Y., Russell, M. P., Benevides, J. M., and Thomas, G. J., Jr. (1997) Raman and infrared spectra of (2′*S*)-[2′-^{2}H]thymidine: Vibrational coupling between deoxyribosyl and thymine moieties and structural implications, *J. Am. Chem. Soc. 119*, 2025−2032.
54. Thomas, G. J., Jr., Benevides, J. M., and Prescott, B. (1986) DNA and RNA structures in crystals, fibers and solutions by Raman spectroscopy with applications to nucleoproteins, in *Biomolecular Stereodynamics* (Sarma, S., and Sarma, A., Eds.) Vol. IV, pp 227−253, Adenine Press, Guilderland, NY.

55. Jerkovic, B., and Bolton, P. H. (2000) The curvature of dA tracts is temperature dependent, *Biochemistry 39*, 12121−12127.
56. Benevides, J. M., Kukolj, G., Autexier, C., Aubrey, K. L., DuBow, M. S., and Thomas, G. J., Jr. (1994) Secondary structure and interaction of phage D108 Ner repressor with a 61-base-pair operator: Evidence for altered protein and DNA structures in the complex, *Biochemistry 33*, 10701−10710.
57. Sun, D., Hurley, L. H., and Harshey, R. M. (1996) Structural distortions induced by integration host factor (IHF) at the H′ site of phage λ probed by (+)-CC-1065, pluramycin, and $KMnO_4$ and by DNA cyclization studies, *Biochemistry 35*, 10815−10827.
58. Pil, P. M., Chow, C. S., and Lippard, S. J. (1993) High-mobility-group 1 protein mediates DNA bending as determined by ring closures, *Proc. Natl. Acad. Sci. U.S.A. 90*, 9465−9469.

BI0523557